

Room-temperature tuning of magnetic anisotropy in samarium-thulium orthoferrites

Juan P. Bolletta ^{1,*}, Gabriel J. Cuello ², Vivian Nassif,³ Emmanuelle Suard,² Alexander I. Kurbakov ⁴,
Antoine Maignan ¹, Christine Martin ¹ and Raúl E. Carbonio⁵

¹Laboratoire CRISMAT, Normandie Université, ENSICAEN, UNICAEN, CNRS, 14050 Caen, France

²Institut Laue Langevin (ILL), 38042 Grenoble, France

³Université Grenoble Alpes, CNRS, Institut Néel, 38000 Grenoble, France

⁴NRC «Kurchatov Institute» - PNPI, 188300 Gatchina, Russia

⁵INFIQC (Consejo Nacional de Investigaciones Científicas y Técnicas [CONICET]–Universidad Nacional de Córdoba),
Departamento de Fisicoquímica, Facultad de Ciencias Químicas,
Universidad Nacional de Córdoba, X5000HUA Córdoba, Argentina



(Received 14 September 2021; accepted 25 January 2022; published 9 February 2022)

Rare-earth orthoferrites ($R\text{FeO}_3$) provide a flexible playground for magnetic materials design, combining the magnetic properties arising from complex interactions between R^{3+} and Fe^{3+} cations within the robust framework of the perovskite structure. The most important magnetic property common to most orthoferrites is a spin reorientation transition in which the magnetic moments of Fe^{3+} cations rotate with respect to a crystallographic axis. SmFeO_3 is unique among orthoferrites due to its high-temperature spin reorientation. It is possible to tune the spin reorientation transition to occur at room temperature by replacing Sm with Tm in the $\text{Sm}_{0.70}\text{Tm}_{0.30}\text{FeO}_3$ perovskite. In this study, we show how small changes in composition in the $\text{Sm}_{1-x}\text{Tm}_x\text{FeO}_3$ ($x = 0.30\text{--}0.50$) series provide a high degree of control over the magnetic properties. This work also offers a rather unusual look into the magnetic structure of a samarium-based perovskite by means of neutron powder diffraction, which was made possible by using ^{152}Sm . The combination of these results and magnetization measurements allowed the construction of the magnetic phase diagram of the series.

DOI: [10.1103/PhysRevB.105.054407](https://doi.org/10.1103/PhysRevB.105.054407)

I. INTRODUCTION

Rare-earth orthoferrites ($R\text{FeO}_3$) have been studied extensively for a long time, in part due to their outstanding magnetic properties, which include magnetodielectricity [1,2], magnetocaloric effects [3–5], negative magnetization [6–8], and complex magnetic structures [9]. In these perovskites, the magnetic moments of the Fe^{3+} cations adopt an antiferromagnetic (AFM) ordering along one crystallographic axis with a slight canting that produces a net magnetic moment in a different direction, which is referred to as weak ferromagnetism (WFM) [10]. This AFM ordering is mainly caused by the AFM $\text{Fe}^{3+}\text{--O}^{2-}\text{--Fe}^{3+}$ superexchange interaction, while the canting of the Fe^{3+} magnetic moments has been generally ascribed to the antisymmetric Dzyaloshinskii-Moriya exchange interaction [11], although recent studies suggest that single-ion anisotropy may play a larger role than previously thought [12]. Under certain conditions, the magnetic moments can rotate with respect to a crystallographic axis while retaining their relative orientations, in a transition known as spin reorientation (SR). When R^{3+} is a paramagnetic cation, this transition is ascribed to a change in the magnetic anisotropy generated by R^{3+} cations around Fe^{3+} cations. SR transitions can be the product of a change in temperature, as magnetization of the R^{3+} cations increases with decreasing

temperature [13], but it can also be induced by an external magnetic field [14,15] or even by a laser pulse [16]. Given the growing interest in anisotropy control of AFM materials for applications in memory and spintronics devices [17–19], the search for relevant transitions related to magnetic anisotropy at room temperature is an attractive field of research. In this context, rare-earth orthoferrites are also promising candidates for ultrafast order parameter manipulation and spin-current generation [20]. Moreover, some orthoferrites have already been considered for information storage applications thanks to their complex magnetic properties [21–23].

When discussing spin reorientation in orthoferrites, SmFeO_3 quickly stands out. This perovskite has a T_N between 670 and 680 K in which the magnetic moments of the Fe^{3+} substructure order antiferromagnetically in a G -type order along the x axis [9,11,24,25] (G_x , in Bertaut's notation [26]). This component of the magnetic structure is a base vector of the Γ_4 irreducible representation of the $Pbnm$ space group, which also allows an F -type ordering (ferromagnetic) along the z axis and an A -type ordering (AFM) along the y axis [26]. This type of magnetic order is common to all orthoferrites at high temperatures [9]. In SmFeO_3 the magnetic moments of the Fe^{3+} substructure gradually rotate towards the c axis into a G_z configuration, a base vector of the Γ_2 irreducible representation, which also allows a ferromagnetic F_x component and an AFM C_y component [11,26]. SmFeO_3 has an unusually high SR temperature, occurring above room temperature between 450 and 480 K [9,11,25,27]. This transition takes

*Corresponding author: juan-pablo.bolletta@ensicaen.fr

place at higher temperatures than in other related orthoferrites, which usually display SR transitions below 150 K [9]. This high SR temperature can be tuned to room temperature by partially replacing samarium in SmFeO_3 with another rare earth, as demonstrated for praseodymium [28], europium [29], gadolinium [30], terbium [31], dysprosium [32,33], erbium [23,34], and yttrium [9]. Recently, thulium has been added to the list of possible substituents of samarium, achieving a room-temperature SR in $\text{Sm}_{0.70}\text{Tm}_{0.30}\text{FeO}_3$ [35]. The ability to tune this transition does not seem to be intrinsically related to the magnetic characteristics of R^{3+} , since the SR tuning can also be achieved with substitution by Y^{3+} , a diamagnetic cation [9]. This suggests that the main cause of the change in the transition temperature is an overall weakening in the $\text{Sm}^{3+}\text{-Fe}^{3+}$ exchange interactions across the material due to their lower number [28,30]. In all cases, the SR transition temperature decreases with respect to that of SmFeO_3 in an approximately linear manner with increasing R^{3+} content, although the exact trend presents slight variations depending on the identity of R^{3+} [30,31,33]. Thus, the exact composition $\text{Sm}_{1-x}\text{R}_x\text{FeO}_3$ that will produce a SR transition at room temperature will ultimately depend on R^{3+} .

In this study, we explore the fine tuning of SR transitions by substituting Sm^{3+} with Tm^{3+} in the $\text{Sm}_{1-x}\text{Tm}_x\text{FeO}_3$ perovskite within small x intervals, obtaining $\text{Sm}_{1-x}\text{Tm}_x\text{FeO}_3$ perovskites with $x = 0.30, 0.35, 0.40, 0.45,$ and 0.50 . In this way, the SR transition can be meticulously controlled and set to a specific temperature in the vicinity of room temperature. For a deeper understanding of this particular SR transition, we studied the $\text{Sm}_{0.70}\text{Tm}_{0.30}\text{FeO}_3$ perovskite in detail by a combination of magnetization studies and neutron powder diffraction (NPD). In addition, we studied the magnetoelectric properties of the $\text{Sm}_{0.70}\text{Tm}_{0.30}\text{FeO}_3$ perovskite at low temperatures.

II. EXPERIMENT

A. Synthesis

$\text{Sm}_{1-x}\text{Tm}_x\text{FeO}_3$ ($x = 0.30, 0.35, 0.40, 0.45,$ and 0.50) samples were prepared starting from a precursor obtained by a wet chemical route. Stoichiometric amounts of Sm_2O_3 (99.9+%, STREM), Tm_2O_3 (99.9+%, STREM), and $\text{Fe}(\text{NO}_3)_3 \cdot 9\text{H}_2\text{O}$ (99.999+%, STREM) were dissolved in a mixture of nitric and citric acid. By producing a reactive precursor from a solution, a random distribution of the cations is facilitated, as observed in previous syntheses of related perovskites [36,37]. The solution was slowly evaporated, leading to a gel that turns into dry flakes with further evaporation. This product was dried and decomposed at 600°C in air for 12 h. The resulting precursor was ground, pressed into pellets, and heated at 1050°C in air for 12 h. The final product was a brown-orange powder in all cases.

Natural Sm is unsuitable for diffraction with thermal neutrons due to its very high absorption cross-section (5922 ± 56 b for neutrons with $\lambda = 1.798 \text{ \AA}$ [38]). Possible solutions to this issue include diffraction at much shorter wavelengths [39], dilution [40], or isotopic substitution [41]. This latter approach was chosen since either short wavelengths or dilutions would hinder the study of the magnetic structure. For this

reason, a sample of $^{152}\text{Sm}_{0.70}\text{Tm}_{0.30}\text{FeO}_3$ was synthesized replacing natural Sm for the ^{152}Sm isotope (with an absorption cross section 206 ± 6 b [38]). This was achieved by using isotopically pure $^{152}\text{Sm}_2\text{O}_3$ (Isotope JSC – ROSATOM) as a reagent while following the procedure detailed above.

B. Sample characterization

X-ray powder diffraction (XRPD) patterns were collected at room temperature in a PANalytical X'Pert Pro diffractometer, equipped with a PIXcel detector and a Co source. Neutron powder diffraction (NPD) patterns were obtained for $^{152}\text{Sm}_{0.70}\text{Tm}_{0.30}\text{FeO}_3$ in experiments carried out in the D1B and D2B instruments at the Institut Laue Langevin (ILL) [42–44]. The powder sample was placed in a cylindrical vanadium container. Diffraction patterns were collected with $\lambda = 2.5285 \text{ \AA}$ in the $0.77^\circ\text{--}128.67^\circ$ 2θ range in the D1B instrument, and with $\lambda = 1.5946 \text{ \AA}$ in the $0.00^\circ\text{--}159.95^\circ$ 2θ range in the D2B instrument. For temperature control, a cryofurnace was used for measurements between 1.5 and 450 K in the D1B instrument, and furnaces were used for measurements between RT and 700 K in both D1B and D2B. Diffraction patterns were collected at selected temperatures as well as in dynamic conditions while heating and cooling between 1.5 and 700 K. The analysis of diffraction data was performed by means of the Rietveld method [45] with the FULLPROF software [46,47]. The BASIREPS software [48] was used to perform a symmetry-based representation analysis to help in the determination and study of magnetic structures.

Magnetic measurements were performed using a MPMS-XL SQUID magnetometer (Quantum Design) on pressed powder in capsules, warming from 5 to 400 K in zero-field-cooling and field-cooling (ZFC-FC) modes with an applied magnetic field $H = 100$ Oe. Additional FC magnetization curves were measured with $H = 500, 1000, 2000,$ and 5000 Oe. Isothermal magnetization curves were measured between $+5$ and -5 T at different temperatures for each sample. Additional isothermal magnetization curves were measured for $\text{Sm}_{0.70}\text{Tm}_{0.30}\text{FeO}_3$ between $+9$ and -9 T at 8, 16, and 50 K in a PPMS (Quantum Design) in VSM mode.

Electrical properties measurements were performed on a thin circular platelet of sintered $\text{Sm}_{0.70}\text{Tm}_{0.30}\text{FeO}_3$ [3.59(1) mm diameter and 0.28(1) mm thickness]. Both flat surfaces of the platelet were coated with silver paste to form two parallel electrical contacts. Copper wires were attached to each contact and soldered to the sample holder, which also holds the platelet standing on its curved face, adhered with electrically insulating GE varnish. These wires were soldered to a sample holder and inserted into a PPMS (Quantum Design) to measure the dielectric constant at low temperature as a function of temperature and applied magnetic field, using an Agilent 4384A LCR meter. The magnetic field varied between -9 and $+9$ T and was applied in the direction parallel to the coated flat surfaces of the sample.

III. RESULTS AND DISCUSSION

Room-temperature XRPD data analysis shows that the structure of these perovskites can be described within the $Pbnm$ (62) space group. In this structure, schematized in

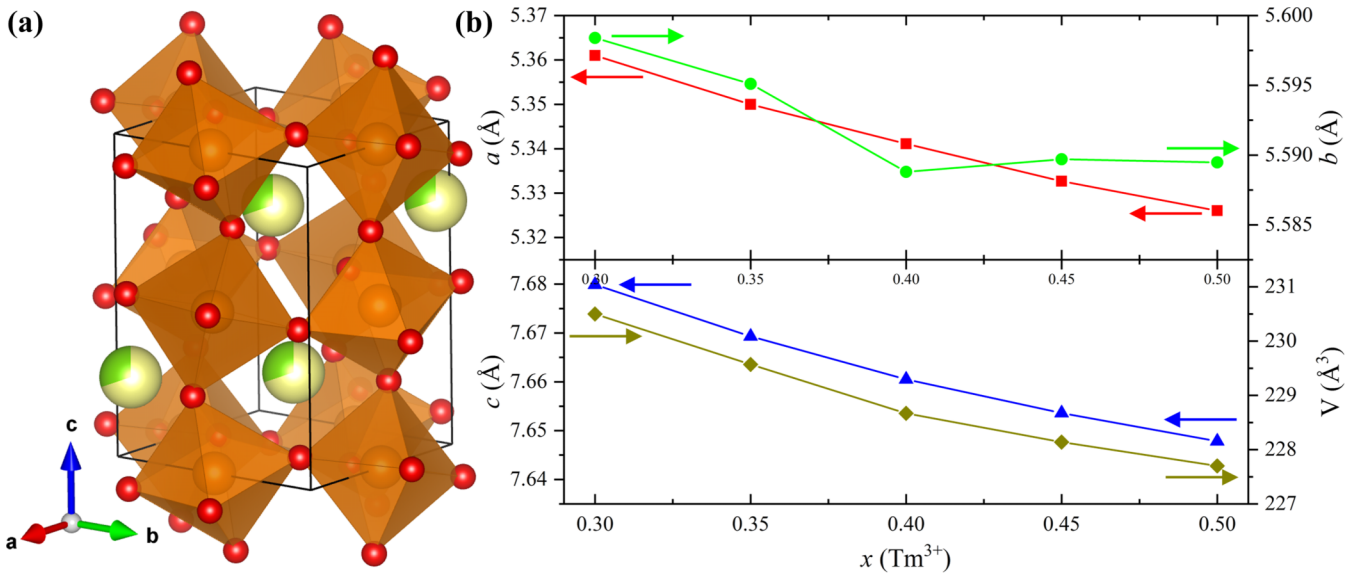


FIG. 1. (a) Crystal structure for $\text{Sm}_{1-x}\text{Tm}_x\text{FeO}_3$, highlighting the FeO_6 octahedra. Yellow and green spheres: Sm^{3+} and Tm^{3+} cations. Orange spheres and octahedra: Fe^{3+} cations. Red spheres: O^{2-} anions. (b) Unit cell parameters and volume vs Tm^{3+} content (x).

Fig. 1(a), Sm^{3+} and Tm^{3+} cations are randomly distributed over a $4c$ ($x, y, 1/4$) site, while Fe^{3+} cations occupy the $4b$ ($1/2, 0, 0$) site. Each iron cation is octahedrally coordinated by six O^{2-} anions, which occupy two different Wyckoff sites: a $4c$ ($x, y, 1/4$) site and an $8d$ (x, y, z) site. The progressive replacement of samarium by thulium causes a contraction of cell parameters and unit cell volume (V), as shown in Fig. 1(b). This is expected due to the smaller radius of Tm^{3+} [effective ionic radii for coordination nine being $r(\text{Sm}^{3+}) = 1.132 \text{ \AA}$ versus $r(\text{Tm}^{3+}) = 1.052 \text{ \AA}$ [49]]. a and c parameters show a steady decrease with increasing Tm^{3+} content, as does the volume V . The b parameter, on the other hand, has a less defined trend and remains roughly constant, varying less than 0.18%. These behaviors are similar to those reported for the $\text{Sm}_{1-x}\text{Tm}_x\text{FeO}_3$ series [35], and also in the related $\text{Sm}_{1-x}\text{Gd}_x\text{FeO}_3$ [50] and $\text{Sm}_{1-x}\text{Dy}_x\text{FeO}_3$ [33]. The variation of cell parameters also matches the general tendencies observed in $R\text{FeO}_3$ perovskites as a function of $r(R^{3+})$, considering $r(R^{3+})$ as the weighted average between Sm^{3+} and Tm^{3+} radii [49]. The $^{152}\text{Sm}_{0.70}\text{Tm}_{0.30}\text{FeO}_3$ sample was also characterized by XRPD and it was found to be indistinguishable from $^{\text{nat}}\text{Sm}_{0.70}\text{Tm}_{0.30}\text{FeO}_3$ samples.

Magnetization versus temperature curves in ZFC and FC modes with $H = 100 \text{ Oe}$ are shown in Fig. 2 for all samples in the series. In all cases, the T_N corresponding to the AFM ordering of the Fe^{3+} substructure is above the higher-temperature limit of the magnetization experiments (400 K), in line with previous observations for orthoferrites [9]. The magnetization curves of these perovskites display common features with noticeable shifts in the transition temperatures. Magnetization in orthoferrites can be understood as a combination of the net WFM moment of the Fe^{3+} substructure and the contribution of the rare-earth cations. Rare-earth cations usually have a mainly paramagnetic behavior and are highly influenced by the effective magnetic field originated from the transition metal WFM, with a lesser contribution from a weak

exchange interaction with the Fe^{3+} cations [11,25,51]. The overall shape of the ZFC magnetization curves is very similar regardless of composition, displaying a gradual increase in magnetization as temperature decreases interrupted by a drop, followed by another gradual increase at lower temperatures. The distinctive drop in the magnetization curves in ZFC mode has been associated with the temperature region in which the SR transition takes place in both SmFeO_3 [24,27,35] and TmFeO_3 [1,52], as well as in other orthoferrites [9,33]. To delimit the temperatures of the transition, the temperature of minimum magnetization below the drop and the temperature of maximum magnetization above the drop have been designated as T_{SR1} and T_{SR2} , respectively. These temperatures are indicated in Fig. 2 for two of the perovskites, and are considered boundaries for the beginning and end of the SR transition. It is also possible to determine a T_{SR} value, defined as the temperature for the inflection point in the magnetization curves across the SR transition, readily observed as a maximum in the first derivatives of these curves. The derivative curves are included in Fig. SM1 [53], together with markers indicating T_{SR1} , T_{SR} , and T_{SR2} . It becomes evident that the changes in composition are producing a shift in the SR temperatures. At higher Tm contents, the transition moves towards lower temperatures, affecting T_{SR1} , T_{SR} , and T_{SR2} . For example, the SR transition can be tuned to have its middle point at RT ($T_{SR} = 301 \text{ K}$) for $\text{Sm}_{0.70}\text{Tm}_{0.30}\text{FeO}_3$, to begin slightly below RT ($T_{SR2} = 289 \text{ K}$) for $\text{Sm}_{0.60}\text{Tm}_{0.40}\text{FeO}_3$, or to happen completely below RT for higher Tm content. Figure 3(a) reflects the variation of the different SR temperatures with x for all the $\text{Sm}_{1-x}\text{Tm}_x\text{FeO}_3$ perovskites, outlining a magnetic phase diagram. Small changes in composition produce noticeable shifts in both T_{SR1} and T_{SR2} , as the incorporation of Tm^{3+} reduces the number of Sm^{3+} - Fe^{3+} interactions [31,33]. The SR temperature decrease correlates with the change in composition in an almost linear way, which constitutes an important tool for the tuning of the SR transition on itself.

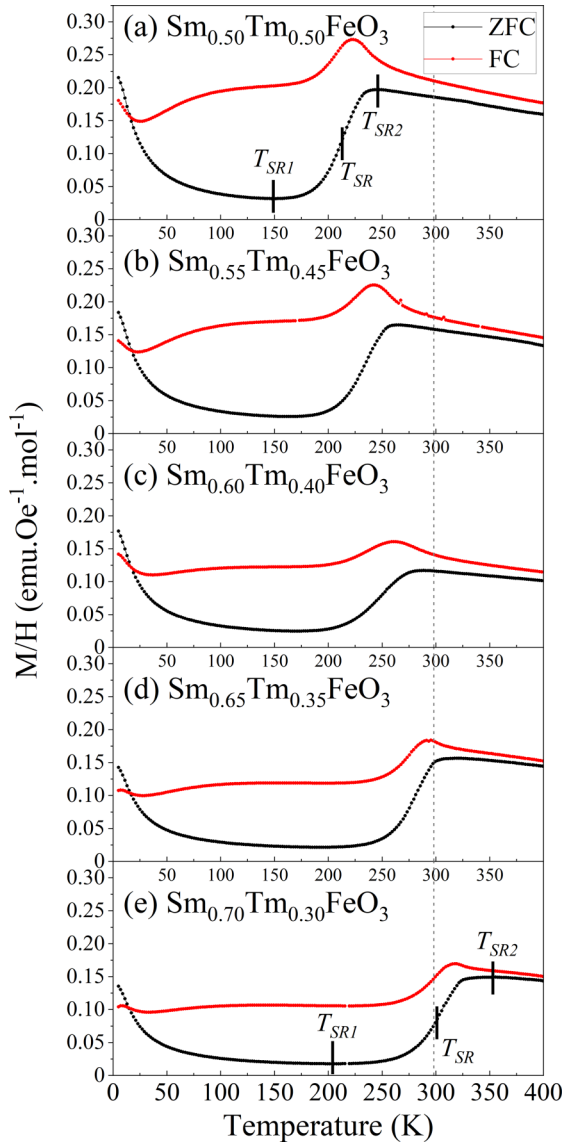


FIG. 2. Magnetization vs temperature curves for $\text{Sm}_{1-x}\text{Tm}_x\text{FeO}_3$ in both ZFC and FC modes ($H = 100$ Oe). Dashed line corresponds to room temperature (298 K).

Magnetization measurements versus an applied magnetic field were performed as a way to further probe the magnetic properties of these materials, particularly in the surroundings of the SR transition. The curves for $\text{Sm}_{0.70}\text{Tm}_{0.30}\text{FeO}_3$ are displayed in Fig. 3(b). Hysteresis loops are observed at temperatures close to the frontiers of the SR transition at 200, 250, and 350 K, with different loop shapes but similar coercive fields (H_c) and remnant magnetizations. These small loops are evidence of a WFM contribution due to a net F component of the canted Fe^{3+} magnetic moments. As detailed below, this is compatible with the characteristic $F_x C_y G_z (\Gamma_2) - G_x A_y F_z (\Gamma_4)$ SR transition described for many orthoferrites, where both magnetic phases allow a net FM component in the transition metal substructure. The small hysteresis loops appear superimposed with the paramagnetic contribution of the R^{3+} cations. At 300 K $\approx T_{SR}$, a thinner hysteresis loop is observed, with a notably lower H_c . This indicates a lower

overall anisotropy during the reorientation, facilitating the orientation of magnetic moments by the applied magnetic field, as observed in SR transitions of other orthoferrites [29,54,55]. Similar results are obtained in the other samples of the family with the corresponding temperature shifts. The H_c extracted from multiple $M(H)$ curves at different temperatures before, during, and after the SR transition for all samples are mapped in a contour plot included in the background of the magnetic phase diagram shown in Fig. 3, while the corresponding H_c values are supplied in Table SM1 [53]. In this schematic visualization, the boundaries of the SR transition also outline magnetic phases displaying a higher magnetic anisotropy, reflected as a higher H_c , which decreases approaching T_{SR} in the middle point of the transition. In this way, T_{SR} represents a valuable point in the phase diagram that indicates a state of minimum coercivity and thus lower magnetic anisotropy, which means that the tuning of the SR transition can be extended to the tuning of the magnetic anisotropy of these materials.

To complete the characterization of this room-temperature magnetic transition on $\text{Sm}_{0.70}\text{Tm}_{0.30}\text{FeO}_3$, its magnetic structure was studied with NPD. Given the large difference in scattering lengths for ^{152}Sm (-5.0 ± 6 fm) and $^{\text{nat}}\text{Tm}$ (7.07 ± 3 fm) [38], it was possible to determine the stoichiometry by refining the occupation of each cation in the R^{3+} ($4c$) site, leading to $^{152}\text{Sm}_{0.71(1)}\text{Tm}_{0.29(1)}\text{FeO}_3$, within experimental error of the intended stoichiometry. Oxygen content was also refined, and no deviations were observed from the stoichiometric value. Three diffraction patterns (at $T = 700, 450,$ and 1.5 K) are shown in Fig. 4, together with their corresponding Rietveld refinements. At 700 K, $\text{Sm}_{0.70}\text{Tm}_{0.30}\text{FeO}_3$ is paramagnetic, with no contributions from any long-range magnetic structure. NPD measurements performed in a broad temperature range allowed for the determination of cell parameters versus temperature, as shown in Fig. 5. There is a steady contraction of all cell parameters with decreasing temperatures. This follows an approximately linear trend for a wide range of temperatures, as observed for SmFeO_3 [40]. The a parameter reaches a plateau below 125 K, while b and c do so below ≈ 50 K. No evidence of structural transitions or superstructures was observed in the explored temperature range. NPD experiments also allowed the determination of the high-temperature T_N of $\text{Sm}_{0.70}\text{Tm}_{0.30}\text{FeO}_3$, which lies at 652 K. This is the temperature at which peaks corresponding to the (011) and (101) reflections from the magnetic structure (also signaled in Fig. 4) first appear, as can be seen in the diagram presented in Fig. 6. Both of these peaks become more intense as temperature decreases. The magnetic structure between 652 and 400 K determined by Rietveld analysis of NPD data is a $G_x (\Gamma_4)$ ordering of the magnetic moments of the Fe^{3+} substructure, which is schematized in Fig. 7.

When comparing Figs. 4(b) and 4(c), a change in the relative intensities of the first two peaks in the diffraction pattern, i.e., the (011) and (101) reflections, is observed, corresponding to the rotation of the magnetic moments of the Fe^{3+} substructure in the SR transition. In fact, the magnetic structure at 1.5 K [Fig. 4(c)] corresponds to a $G_z (\Gamma_2)$ ordering, also schematized in Fig. 7. To characterize this SR transition in detail, diffraction patterns were collected while heating the sample between 1.5 and 450 K, as shown in

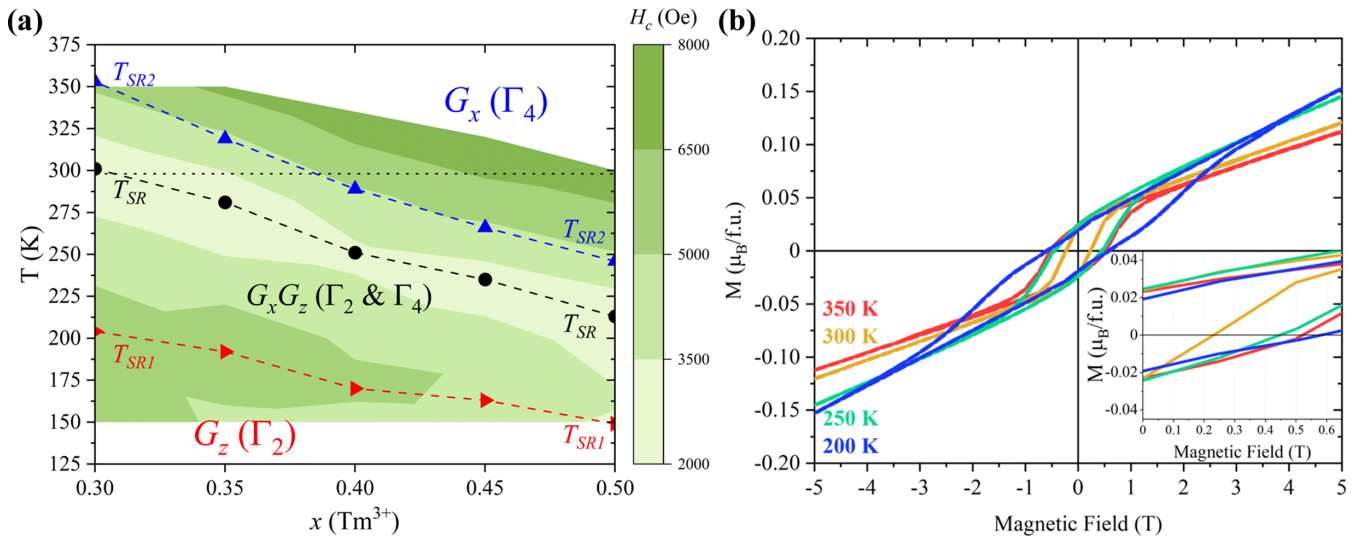


FIG. 3. (a) Temperature boundaries (T_{SR1} and T_{SR2}) and middle point (T_{SR}) of the spin reorientation transition vs Tm^{3+} content in $\text{Sm}_{1-x}\text{Tm}_x\text{FeO}_3$ from magnetometry, along with a schematic mapping of H_c values in the background. Magnetic structure types derived from NPD for $\text{Sm}_{0.70}\text{Tm}_{0.30}\text{FeO}_3$ are also indicated. (b) Magnetization vs applied magnetic field for $\text{Sm}_{0.70}\text{Tm}_{0.30}\text{FeO}_3$. Inset: low magnetic field region to visualize H_c .

Fig. 8 in the range of temperatures corresponding to SR. The (101) peak becomes stronger with decreasing temperature, while the (011) reflection decreases. Below 205 K, these two peaks have very similar intensities, and Rietveld analysis of the diffraction patterns indicates a $G_z(\Gamma_2)$ ordering down to 1.5 K. The diffraction pattern collected at 1.5 K shows no

additional peaks, and all intensities are correctly calculated using a magnetic and nuclear structure model that does not consider a magnetic contribution of the R^{3+} cations or any additional components in the magnetic moments of the Fe^{3+} substructure. This excludes possible long-range magnetic ordering of the magnetic moments of lanthanides in

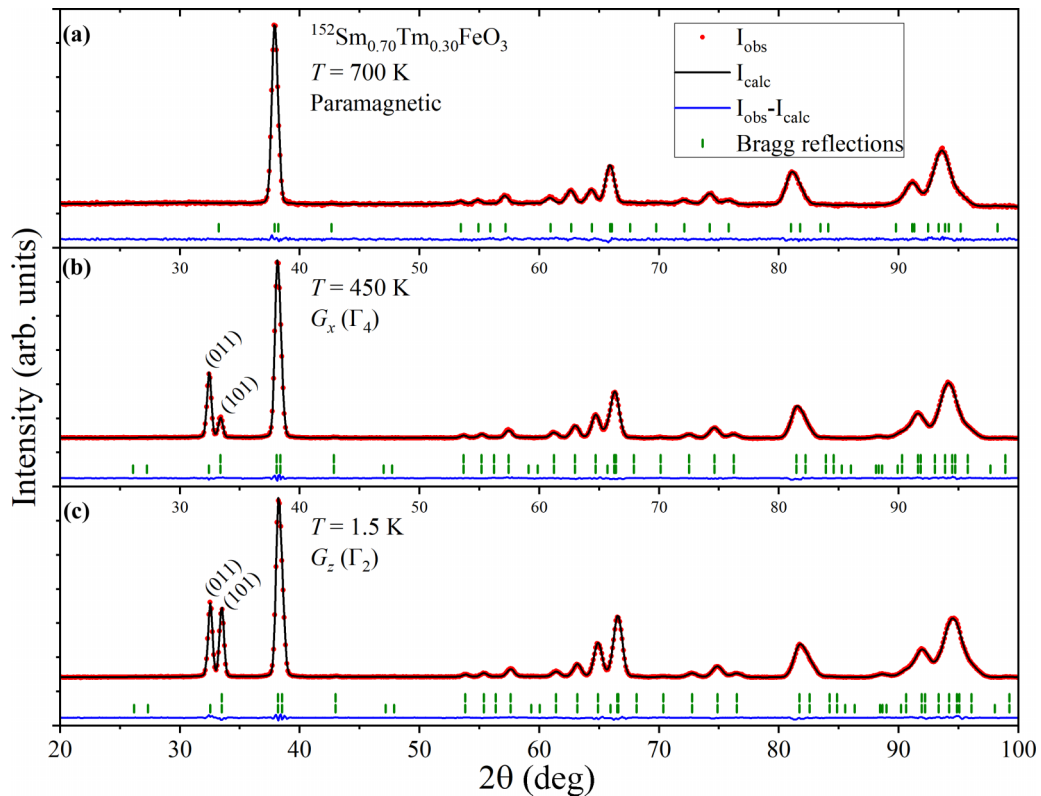


FIG. 4. NPD patterns obtained in the D1B instrument for $^{152}\text{Sm}_{0.70}\text{Tm}_{0.30}\text{FeO}_3$ at $T = 700$ K (a), 450 K (b), and 1.5 K (c). First row of Bragg reflections: nuclear structure. Second row: magnetic structure. Blue curves show the difference between experimental and calculated NPD patterns.

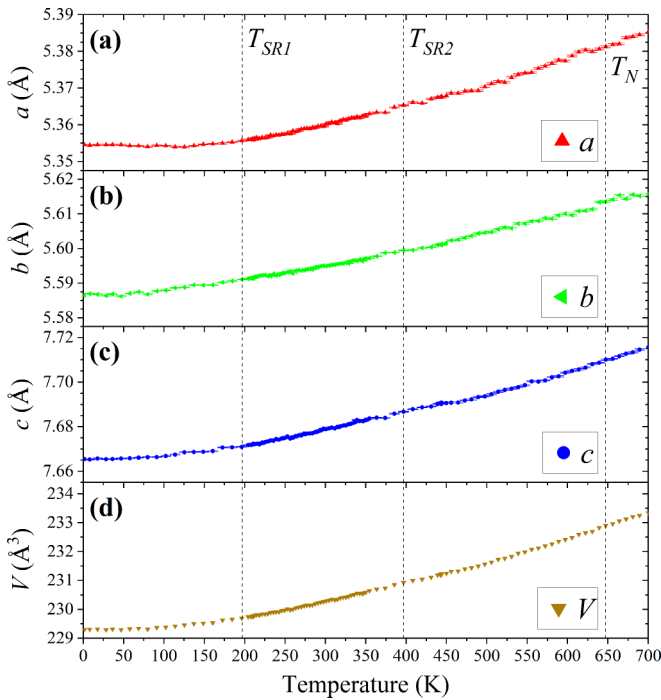


FIG. 5. Cell parameters (a)–(c) and unit cell volume (d) vs temperature for $^{152}\text{Sm}_{0.70}\text{Tm}_{0.30}\text{FeO}_3$ obtained from NPD experiments. Dashed lines indicate Néel temperature and boundaries of the SR transition obtained from NPD experiments.

$\text{Sm}_{0.70}\text{Tm}_{0.30}\text{FeO}_3$, contrary to previous asseverations [35]. The total refined magnetic moment for the Fe^{3+} ions at low temperatures is close to $4.1\mu_B$, lower than the $5\mu_B$ expected for a free Fe^{3+} ion, but in accordance with other reports of NPD in orthoferrites [56,57].

The individual diffraction patterns that compose the diagrams shown in Figs. 6 and 8 were integrated and analyzed by the Rietveld method, extracting the x and z magnetic components of the Fe^{3+} cations. The results are shown in Fig. 9 along with the corresponding ZFC magnetization curve ($H = 100$ Oe). This figure represents the behavior of the magnetic moment of the bottom-left Fe^{3+} cation in the magnetic structures shown in Fig 7, positioned at $(1/2, 0, 0)$. The neighboring Fe^{3+} cations will adopt the same magnitude for the components of their magnetic moments but with relative orientations defined by the G -type AFM magnetic ordering.

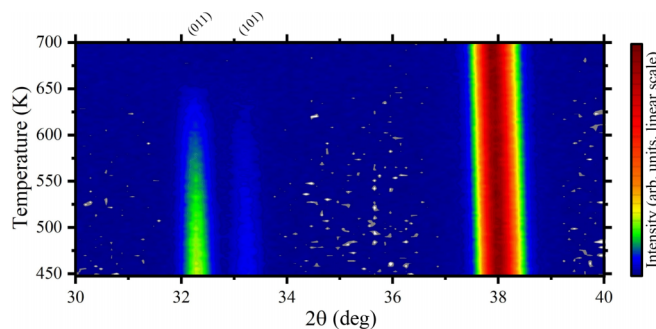


FIG. 6. Temperature-dependent NPD for $^{152}\text{Sm}_{0.70}\text{Tm}_{0.30}\text{FeO}_3$ between 450 and 700 K obtained in the D1B instrument.

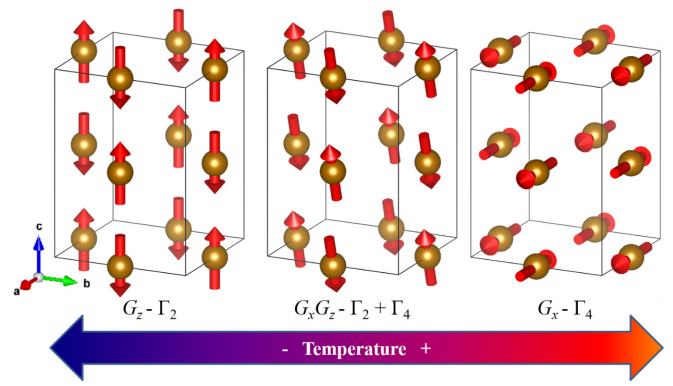


FIG. 7. Schematic representation of the SR transition between G_z (Γ_2) and G_x (Γ_4) magnetic structures in the transition metal substructure of an orthorhombic perovskite.

There was no evidence of other Fe^{3+} magnetic moment components in the NPD data within the detection limits of the experiments, although a WFM component in the Fe^{3+} substructure can be inferred above and below the SR transition from the small hysteresis loops observed in the magnetization versus applied magnetic field shown in Fig. 3, as mentioned above. As temperature decreases, there is a gradual rotation of the Fe^{3+} magnetic moments from the x direction to the z direction that takes place across a wide range of temperatures, from 210 to 390 K. The x component decreases with the temperature, while the component in the z direction increases. During the transition, the Fe^{3+} magnetic moments keep their relative G -type ordering in both directions, making it a G_x - G_z SR transition, which is also schematized in Fig. 7. This type of rotation is also reported for SmFeO_3 and TmFeO_3 [9,25,58]. The rotation is closely correlated to the drop in magnetization in the ZFC magnetization curve also shown in Fig. 9. The SR has its middle point almost at room temperature, which also matches the middle point of the magnetization drop (T_{SR}). The low-temperature boundary of this gradual rotation (T_{SR1}) is in good accordance with the estimates performed over the magnetization curves, while the high-temperature boundary determined by NPD ($T_{SR2,NPD}$) occurs at higher temperatures than the temperature of the maximum in the magnetization curve (T_{SR2}). The SR takes place in an unusually wide range of temperatures spanning over 180 K, which, compared to other reports on orthoferrites, may be caused by differences

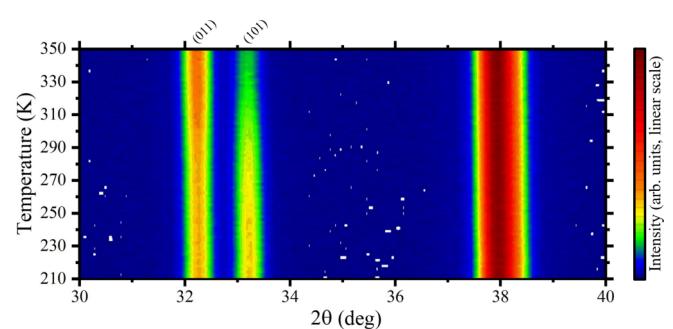


FIG. 8. Temperature-dependent NPD for $^{152}\text{Sm}_{0.70}\text{Tm}_{0.30}\text{FeO}_3$ in the SR temperature region obtained in the D1B instrument.

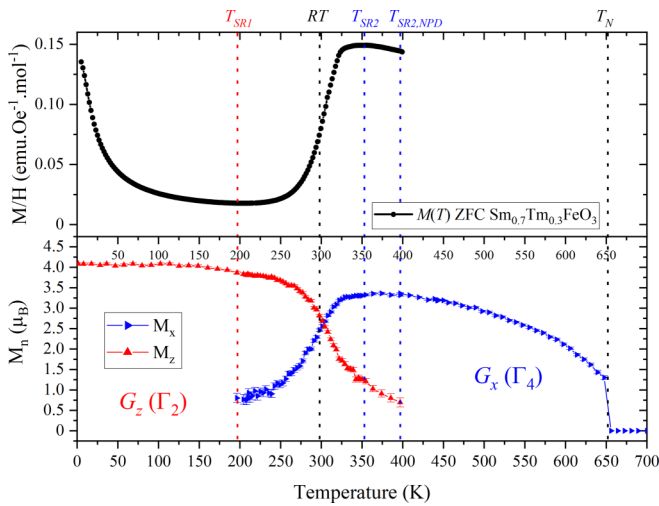


FIG. 9. Upper panel: magnetization vs temperature for $\text{Sm}_{0.70}\text{Tm}_{0.30}\text{FeO}_3$ (ZFC, $H = 100$ Oe). Lower panel: x and z components of the magnetic moment of one Fe^{3+} cation [Fe^{3+} at $(1/2, 0, 0)$, lower left in Fig. 7], in $^{152}\text{Sm}_{0.70}\text{Tm}_{0.30}\text{FeO}_3$ vs temperature. Dashed lines indicate relevant temperatures. In these refinements, the components of the Fe^{3+} magnetic moment do not reach zero at any temperature, but the values are arbitrarily made equal to zero when the relative error of the refined values begins to exceed 20%.

between powder and single-crystal samples [27,59]. Another possible cause is the local change in the magnetic anisotropy

around the Fe^{3+} cations due to a random distribution of the different R^{3+} cations. For example, a similar widening of the SR range has been observed in substituted magnetic alloys with random distributions of magnetic atoms [60]. The different magnetic structures found across the SR transition are also relevant to the construction of the magnetic phase diagram. Given the correspondence between the ZFC curve and the rotation of the Fe^{3+} magnetic moments in $^{152}\text{Sm}_{0.70}\text{Tm}_{0.30}\text{FeO}_3$, and the strong similarities between ZFC curves of all the perovskites in the series, it is possible to extrapolate the magnetic structures with the corresponding changes in SR temperatures, completing the magnetic phase diagram presented in Fig. 3. Considering the progressive and rotational nature of the SR transition, it follows that the value of x will control not only the SR temperature range, but also the specific magnetic structure at every temperature.

To further probe the magnetic behavior of $\text{Sm}_{0.70}\text{Tm}_{0.30}\text{FeO}_3$ at lower temperatures, additional isothermal magnetization measurements versus applied magnetic field were performed at several temperatures, as shown in Fig. 10. When temperature is decreased below 200 K, the hysteresis loops become thinner, being practically nonexistent in the isotherms below 50 K, displaying a behavior similar to a paramagnetic material, with an increasing magnitude of magnetization due to the higher magnetic polarization of the R^{3+} cations at low temperatures. The disappearance of the hysteresis loop can be explained by the magnetic coupling between R^{3+} and the transition metal becoming stronger at lower temperatures, and thus both

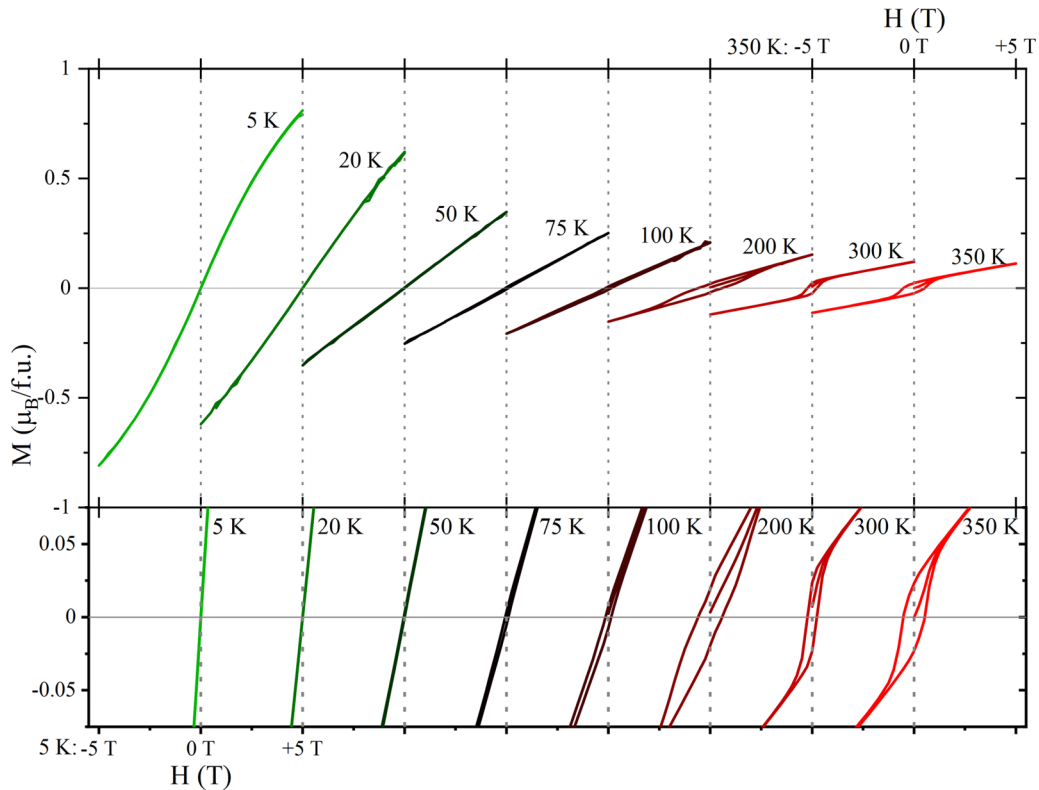


FIG. 10. Magnetization vs applied magnetic field for $\text{Sm}_{0.70}\text{Tm}_{0.30}\text{FeO}_3$. Magnetization cycles measured at different temperatures are offset along the x axis to facilitate visualization and comparison. Scales in the x axis are presented for first and last cycle for reference. Lower panel: detail of the low magnetization region and the WFM loop.

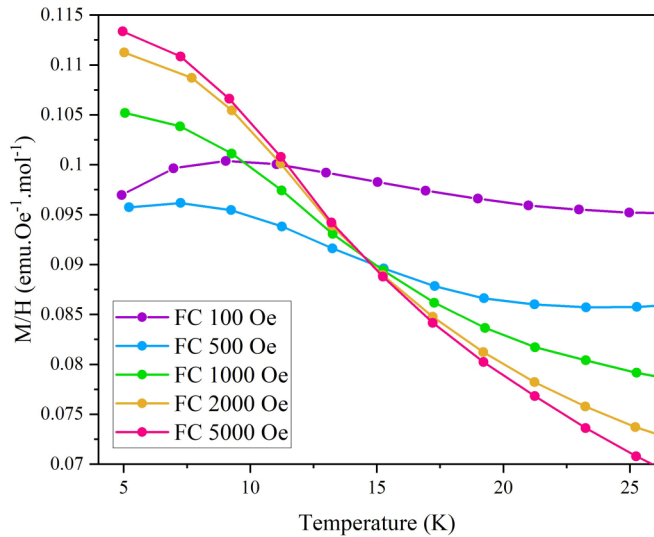


FIG. 11. Detail of the low-temperature region of magnetic susceptibility (M/H) vs temperature in FC mode for $\text{Sm}_{0.70}\text{Tm}_{0.30}\text{FeO}_3$ at different applied magnetic fields.

change their orientations together when a magnetic field is applied, decreasing the coercive field H_c [59,61]. A similar disappearance of the hysteresis loop has also been observed in reports about $\text{Sm}_{0.70}\text{Tm}_{0.30}\text{FeO}_3$ [35], TmFeO_3 [62], and in SmFeO_3 [27,59]. Additionally, magnetization versus temperature curves were measured in FC mode, as shown in Fig. 11. The curve at 500 Oe shows a similar behavior to that at $H = 100$ Oe. Below 100 K, these curves display a decrease in magnetization that can still be appreciated down to ≈ 25 K. This feature differs from the ZFC curves and is associated with the appearance of a FM component in the R^{3+} substructure that becomes AFM coupled to the WFM of Fe^{3+} in SmFeO_3 below 150 K [25,27,59,63]. This coupling would also relate to the thinning and disappearance of the hysteresis loops due to a coordinated behavior as discussed above. Meanwhile, the FC magnetization curves for $H \geq 1000$ Oe display a different behavior, similar to the ZFC curves, with only a subtle decrease in slope at low temperatures. This is evidence of the coupled $\text{Sm}^{3+}\text{-Fe}^{3+}$ magnetic moments rotating as an ensemble due to the applied magnetic field. This is reminiscent of the spin-flip transition observed in SmFeO_3 single crystals, where the $\text{Sm}^{3+}\text{-Fe}^{3+}$ ensemble changes orientation when the crystal is subjected to $H > 2000$ Oe [25]. In a powder sample, where all crystal orientations are represented, this would mean that at high applied magnetic fields the resultant magnetic moment of the $\text{Sm}^{3+}\text{-Fe}^{3+}$ ensemble is pointing in the direction of the applied magnetic field, behaving more like the general paramagnetic dependence of R^{3+} moments with temperature and canceling the negative trend in magnetization displayed at lower magnetic fields. In addition to this, the Tm^{3+} ions will certainly play some role in the complex magnetic behaviors. Tm^{3+} develops a FM component parallel to the WFM of Fe^{3+} in TmFeO_3 due to magnetic dipolar interaction [64]. Assuming that $R^{3+}\text{-}R^{3+}$ interactions in general are weak and only become relevant at very low temperatures, different relative orientations of Sm^{3+} and Tm^{3+} with the Fe^{3+} WFM

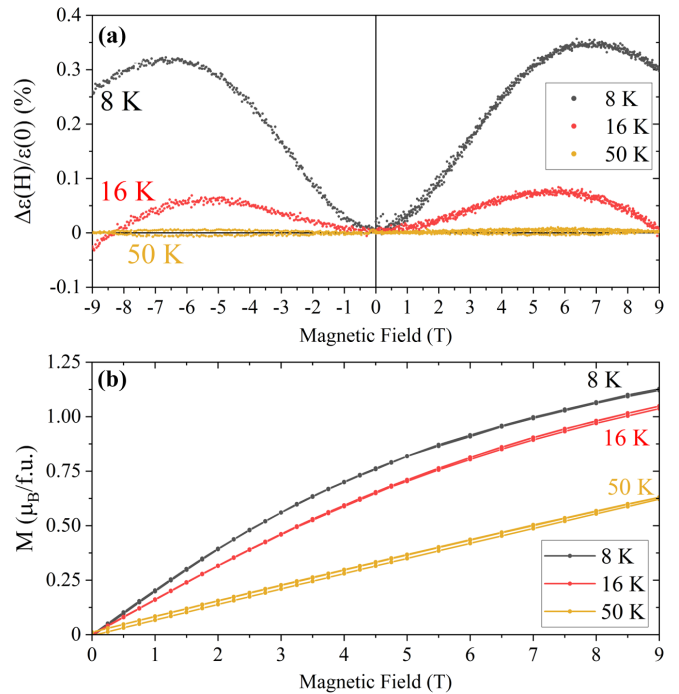


FIG. 12. (a) Magnetodielectric effect (MDE) for $\text{Sm}_{0.70}\text{Tm}_{0.30}\text{FeO}_3$ at 8, 16, and 50 K ($f = 50$ kHz). (b) Magnetization vs applied magnetic field for $\text{Sm}_{0.70}\text{Tm}_{0.30}\text{FeO}_3$ between 0 and 9 T at 8, 16, and 50 K.

moments will produce a competition or compensation effect that could explain the oscillations observed in the FC curves with $H < 1000$ Oe below 25 K.

Dielectric constant measurements were also performed on $\text{Sm}_{0.70}\text{Tm}_{0.30}\text{FeO}_3$ at low temperatures under an applied magnetic field. A small magnetodielectric effect (MDE) was found at 8 K, becoming smaller as temperature is increased to 16 K, and almost nonexistent at 50 K, as shown in Fig. 12(a). A MDE with very similar behavior regarding magnetic field and temperature was observed in TmFeO_3 [1], where a link between the compensation temperature of R^{3+} and Fe^{3+} magnetic moments and the appearance of MDE is proposed, suggesting changes in magnetic anisotropy and magnetostriction as possible factors. In $\text{Sm}_{0.70}\text{Tm}_{0.30}\text{FeO}_3$ there are hints about the complex interplay between Sm^{3+} , Tm^{3+} , and Fe^{3+} magnetic moments that may give rise to these effects. Although no compensation temperature is observed in the different measurements performed, the low-temperature FC curves shown in Fig. 11 hint that these magnetic interactions between the different cations will be disturbed by an increasing magnetic field, as described above. Additional isothermal magnetization curves were measured for $\text{Sm}_{0.70}\text{Tm}_{0.30}\text{FeO}_3$ up to 9 T to replicate the conditions during the dielectric constant measurements, as shown in Fig. 12(b). The curves at 8 and 16 K display an S-shaped closed curve with no hysteresis, previously associated with a strong magnetic coupling between R^{3+} and Fe^{3+} , while the curve at 50 K shows a slightly open loop, suggesting that this coupling is weakening at increasing temperatures. The MDE vanishing with a decreasing $R^{3+}\text{-Fe}^{3+}$ magnetic coupling is in accordance with observations in other related perovskites. The strong magnetic

interaction between R^{3+} and M^{3+} cations that prevails at low temperatures has been proposed as the responsible for MDE in perovskites such as ErCrO_3 and $\text{HoFe}_{0.50}\text{Co}_{0.50}\text{O}_3$, where MDE also decreases with increasing temperature [65,66]. On the other hand, there is no clear correlation between the features of the isothermal magnetization curves shown in Fig. 12(b) and the saturation of MDE, happening approximately between 5.5 and 6.5 T depending on the temperature. Saturation of MDE has also been observed in TmFeO_3 and Mn_3O_4 , although no unique explanation has been offered [1,67]. Further studies are needed to clarify the origin of the MDE, its dependence with temperature, magnetic field, and its implications regarding a possible magnetoelectric coupling in these perovskites.

IV. CONCLUSIONS

The combination of magnetization measurements and NPD data has provided a very detailed insight into the $G_z(\Gamma_2)$ to $G_x(\Gamma_4)$ SR transition of $\text{Sm}_{1-x}\text{Tm}_x\text{FeO}_3$ perovskites. By tuning the composition, the SR below RT for $\text{Sm}_{0.60}\text{Tm}_{0.40}\text{FeO}_3$ (and higher x) evolves to a SR finishing at RT for $\text{Sm}_{0.65}\text{Tm}_{0.35}\text{FeO}_3$ and then to a SR with its middle point exactly at RT for $\text{Sm}_{0.70}\text{Tm}_{0.30}\text{FeO}_3$. The tuning of composition not only achieves specific SR transition temperatures, but also a specific magnetic structure at a certain temperature because of the gradual nature of the SR transition. Magnetization isotherms have allowed us to associate the SR with a marked decrease in the magnetic anisotropy, which means that x also affects this property. This unveils multiple possibilities available for future research in simultaneous control of

magnetization, magnetic structure, and magnetic anisotropy within this range of compositions, temperatures, and magnetic fields. A small MDE effect was also observed at low temperatures for $\text{Sm}_{0.70}\text{Tm}_{0.30}\text{FeO}_3$, which may be related to the complex interplay between Sm^{3+} , Tm^{3+} , and the WFM from Fe^{3+} magnetic moments at low temperatures. Besides the changes in the SR transition temperatures, no other drastic changes in magnetic behavior were observed, which suggests that most of the effects are mainly due to a dilution in the Sm^{3+} - Fe^{3+} exchange interactions by the substitution of Sm^{3+} with Tm^{3+} . For this reason, the observations in this study could be extended to substitutions with other lanthanides in the SmFeO_3 perovskite, providing useful tools and guidelines for the design of oxides with tailored magnetic properties and magnetic structures in the vicinity of room temperature.

ACKNOWLEDGMENTS

J.P.B. thanks CONICET for the scholarship under which this work took place, INFIQC (CONICET-UNC), and ILL for beam time. J.P.B., A.M., and C.M. acknowledge the financial support of the French Agence Nationale de la Recherche LabEx EMC3 through the Project MaPhoOBi (Grant No. ANR-10-LABX-09-01), and the Normandy Region (Réseau d'Intérêt Normand-Label d'Excellence), as well as the helpful assistance of Fabien Veillon with physical measurements. A.I.K. gratefully acknowledges the financial support from Russian Science Foundation via Grant No. 18-02-0326. R.E.C. wants to thank ANPCYT for financial support through project FON-CyT (PICT-2016-2495) and SECYT-UNC for project Res. 190/2021.

-
- [1] R. Muralidharan, T.-H. Jang, C.-H. Yang, Y. H. Jeong, and T. Y. Koo, Magnetic control of spin reorientation and magnetodielectric effect below the spin compensation temperature in TmFeO_3 , *Appl. Phys. Lett.* **90**, 012506 (2007).
- [2] Z. X. Cheng, H. Shen, J. Y. Xu, P. Liu, S. J. Zhang, J. L. Wang, X. L. Wang, and S. X. Dou, Magnetocapacitance effect in nonmultiferroic YFeO_3 single crystal, *J. Appl. Phys.* **111**, 034103 (2012).
- [3] M. Shao, S. Cao, Y. Wang, S. Yuan, B. Kang, and J. Zhang, Large magnetocaloric effect in HoFeO_3 single crystal, *Solid State Commun.* **152**, 947 (2012).
- [4] M. Das, S. Roy, and P. Mandal, Giant reversible magnetocaloric effect in a multiferroic GdFeO_3 single crystal, *Phys. Rev. B* **96**, 174405 (2017).
- [5] P. Sharma, R. Masrour, A. Jabar, J. Fan, A. Kumar, L. Ling, C. Ma, C. Wang, and H. Yang, Structural and magnetocaloric properties of rare-earth orthoferrite perovskite: TmFeO_3 , *Chem. Phys. Lett.* **740**, 137057 (2020).
- [6] Y. K. Jeong, J.-H. Lee, S.-J. Ahn, and H. M. Jang, Temperature-induced magnetization reversal and ultra-fast magnetic switch at low field in SmFeO_3 , *Solid State Commun.* **152**, 1112 (2012).
- [7] S. J. Yuan, W. Ren, F. Hong, Y. B. Wang, J. C. Zhang, L. Bellaiche, S. X. Cao, and G. Cao, Spin switching and magnetization reversal in single-crystal NdFeO_3 , *Phys. Rev. B* **87**, 184405 (2013).
- [8] H. J. Zhao, J. Íñiguez, X. M. Chen, and L. Bellaiche, Origin of the magnetization and compensation temperature in rare-earth orthoferrites and orthochromates, *Phys. Rev. B* **93**, 014417 (2016).
- [9] R. L. White, Review of recent work on the magnetic and spectroscopic properties of the rare-earth orthoferrites, *J. Appl. Phys.* **40**, 1061 (1969).
- [10] R. M. Bozorth, Origin of Weak Ferromagnetism in Rare-Earth Orthoferrites, *Phys. Rev. Lett.* **1**, 362 (1958).
- [11] D. Treves, Studies on orthoferrites at the Weizmann institute of science, *J. Appl. Phys.* **36**, 1033 (1965).
- [12] J.-S. Zhou, L. G. Marshall, Z.-Y. Li, X. Li, and J.-M. He, Weak ferromagnetism in perovskite oxides, *Phys. Rev. B* **102**, 104420 (2020).
- [13] T. Yamaguchi, Theory of spin reorientation in rare-earth orthochromites and orthoferrites, *J. Phys. Chem. Solids* **35**, 479 (1974).
- [14] C. E. Johnson, L. A. Prelorendjo, and M. F. Thomas, Field induced spin reorientation in orthoferrites DyFeO_3 , HoFeO_3 and ErFeO_3 , *J. Magn. Magn. Mater.* **15-18**, 557 (1980).
- [15] Y. B. Bazaliy, L. T. Tsybaly, G. N. Kakazei, A. I. Izotov, and P. E. Wigen, Spin-reorientation in ErFeO_3 : Zero-field transitions, three-dimensional phase diagram, and anisotropy of erbium magnetism, *Phys. Rev. B* **69**, 104429 (2004).

- [16] A. V. Kimel, A. Kirilyuk, A. Tsvetkov, R. V. Pisarev, and T. Rasing, Laser-induced ultrafast spin reorientation in the antiferromagnet TmFeO_3 , *Nature (London)* **429**, 850 (2004).
- [17] I. L. Prejbeanu, S. Bandiera, J. Alvarez-Hérault, R. C. Sousa, B. Dieny, and J.-P. Nozières, Thermally assisted MRAMs: Ultimate scalability and logic functionalities, *J. Phys. D* **46**, 074002 (2013).
- [18] T. Jungwirth, X. Marti, P. Wadley, and J. Wunderlich, Antiferromagnetic spintronics, *Nat. Nanotechnol.* **11**, 231 (2016).
- [19] M. Song, Y. Xu, J. OuYang, Y. Zhang, D. Liu, X. Yang, X. Zou, and L. You, Low current writing perpendicular magnetic random access memory with high thermal stability, *Mater. Design* **92**, 1046 (2016).
- [20] V. Baltz, A. Manchon, M. Tsoi, T. Moriyama, T. Ono, and Y. Tserkovnyak, Antiferromagnetic spintronics, *Rev. Mod. Phys.* **90**, 015005 (2018).
- [21] A. H. Bobeck, Properties and device applications of magnetic domains in orthoferrites, *Bell Syst. Tech. J.* **46**, 1901 (1967).
- [22] A. Bobeck, R. Fischer, A. Perneski, J. Remeika, and L. Van Uitert, Application of orthoferrites to domain-wall devices, *IEEE Trans. Magn.* **5**, 544 (1969).
- [23] A. J. Kurtzig, R. L. Townsend, R. Wolfe, and J. Sosniak, Reorientation and curie point writing in orthoferrites, *J. Appl. Phys.* **42**, 1804 (1971).
- [24] J.-H. Lee, Y. K. Jeong, J. H. Park, M.-A. Oak, H. M. Jang, J. Y. Son, and J. F. Scott, Spin-Canting-Induced Improper Ferroelectricity and Spontaneous Magnetization Reversal in SmFeO_3 , *Phys. Rev. Lett.* **107**, 117201 (2011).
- [25] L. G. Marshall, J.-G. Cheng, J.-S. Zhou, J. B. Goodenough, J.-Q. Yan, and D. G. Mandrus, Magnetic coupling between Sm^{3+} and the canted spin in an antiferromagnetic SmFeO_3 single crystal, *Phys. Rev. B* **86**, 064417 (2012).
- [26] E. F. Bertaut, Representation analysis of magnetic structures, *Acta Crystallogr. A* **24**, 217 (1968).
- [27] C. De, A. K. Nayak, M. Nicklas, and A. Sundaresan, Magnetic compensation-induced sign reversal of exchange bias in a multi-glass perovskite SmFeO_3 , *Appl. Phys. Lett.* **111**, 182403 (2017).
- [28] H. Shen, Q. Xian, T. Xie, A. Wu, M. Wang, J. Xu, R. Jia, and A. M. Kalashnikova, Modulation of magnetic transitions in SmFeO_3 single crystal by Pr^{3+} substitution, *J. Magn. Magn. Mater.* **466**, 81 (2018).
- [29] K. P. Belov, A. M. Kadomtseva, R. Z. Levitin, V. A. Timofeeva, V. S. Uskov, and V. A. Khokhlov, Reorientation of the antiferromagnetic vector of some rare-earth orthoferrites in strong magnetic fields, *JETP* **28**, 1139 (1969).
- [30] R. C. Sherwood, L. G. Van Uitert, R. Wolfe, and R. C. LeCraw, Variation of the reorientation temperature and magnetic crystal anisotropy of the rare-earth orthoferrites, *Phys. Lett. A* **25**, 297 (1967).
- [31] A. Wu, B. Wang, X. Zhao, T. Xie, P. Man, L. Su, A. M. Kalashnikova, and R. V. Pisarev, Crystal growth of $\text{Sm}_{0.3}\text{Tb}_{0.7}\text{FeO}_3$ and spin reorientation transition in $\text{Sm}_{1-x}\text{Tb}_x\text{FeO}_3$ orthoferrite, *J. Magn. Magn. Mater.* **426**, 721 (2017).
- [32] R. D. Pierce, R. Wolfe, and L. G. Van Uitert, Spin reorientation in mixed samarium-dysprosium orthoferrites, *J. Appl. Phys.* **40**, 1241 (1969).
- [33] W. Zhao, S. Cao, R. Huang, Y. Cao, K. Xu, B. Kang, J. Zhang, and W. Ren, Spin reorientation transition in dysprosium-samarium orthoferrite single crystals, *Phys. Rev. B* **91**, 104425 (2015).
- [34] X. Zhao, K. Zhang, K. Xu, P. Man, T. Xie, A. Wu, G. Ma, S. Cao, and L. Su, Crystal growth and spin reorientation transition in $\text{Sm}_{0.4}\text{Er}_{0.6}\text{FeO}_3$ orthoferrite, *Solid State Commun.* **231-232**, 43 (2016).
- [35] A. A. Khan, A. Ahlawat, S. M. Faisal, M. K. Singh, A. K. Karnal, and S. Satapathy, Tuning of spin reorientation temperature of SmFeO_3 by doping of Tm^{3+} ion: Role of exchange interaction between 4f & 3d electrons, *J. Alloy. Compd.* **808**, 151603 (2019).
- [36] F. Pomiro, R. D. Sánchez, G. Cuello, A. Maignan, C. Martin, and R. E. Carbonio, Spin reorientation, magnetization reversal, and negative thermal expansion observed in $\text{RFe}_{0.5}\text{Cr}_{0.5}\text{O}_3$ perovskites ($\text{R} = \text{Lu}, \text{Yb}, \text{Tm}$), *Phys. Rev. B* **94**, 134402 (2016).
- [37] J. P. Bolletta, F. Pomiro, R. D. Sánchez, V. Pomjakushin, G. Aurelio, A. Maignan, C. Martin, and R. E. Carbonio, Spin reorientation and metamagnetic transitions in $\text{RFe}_{0.5}\text{Cr}_{0.5}\text{O}_3$ perovskites ($\text{R} = \text{Tb}, \text{Dy}, \text{Ho}, \text{Er}$), *Phys. Rev. B* **98**, 134417 (2018).
- [38] V. F. Sears, Neutron scattering lengths and cross sections, *Neutron News* **3**, 26 (1992).
- [39] M. Tripathi, R. J. Choudhary, D. M. Phase, T. Chatterji, and H. E. Fischer, Evolution of magnetic phases in SmCrO_3 : A neutron diffraction and magnetometric study, *Phys. Rev. B* **96**, 174421 (2017).
- [40] C.-Y. Kuo, Y. Drees, M. T. Fernández-Díaz, L. Zhao, L. Vasylichko, D. Sheptyakov, A. M. T. Bell, T. W. Pi, H.-J. Lin, M.-K. Wu, E. Pellegrin, S. M. Valvidares, Z. W. Li, P. Adler, A. Todorova, R. Küchler, A. Steppke, L. H. Tjeng, Z. Hu, and A. C. Komarek, $k = 0$ Magnetic Structure and Absence of Ferroelectricity in SmFeO_3 , *Phys. Rev. Lett.* **113**, 217203 (2014).
- [41] A. I. Kurbakov, C. Martin, and A. Maignan, Crystal and magnetic structures and physical properties of the $\text{Sm}_{0.37}\text{Sr}_{0.63}\text{MnO}_3$ manganite, *Phys. Solid State* **50**, 275 (2008).
- [42] R. E. Carbonio, J. G. Cuello, A. Maignan, C. Martin, and V. Nassif, Study of Room-Temperature Spin Reorientation and Low-Temperature Magnetic Structure in $\text{Sm}_{0.7}\text{Tm}_{0.3}\text{FeO}_3$ Perovskite, Institut Laue-Langevin (ILL), Proposal 5-31-2645 (2019) [doi:10.5291/ILL-DATA.5-31-2645].
- [43] J. P. Bolletta and V. Nassif, High-temperature structural studies of $^{152}\text{Sm}_{0.7}\text{Tm}_{0.3}\text{FeO}_3$ perovskite, Institut Laue-Langevin (ILL), Proposal EASY-812 (2021) [doi:10.5291/ILL-DATA.EASY-812].
- [44] J. P. Bolletta and E. Suard, Structural studies of $^{152}\text{Sm}_{0.7}\text{Tm}_{0.3}\text{FeO}_3$ perovskite in the paramagnetic region, Institut Laue-Langevin (ILL), Proposal EASY-811 (2021), doi:10.5291/ILL-DATA.EASY-811.
- [45] H. M. Rietveld, A profile refinement method for nuclear and magnetic structures, *J. Appl. Crystallogr.* **2**, 65 (1969).
- [46] J. Rodríguez-Carvajal, Recent advances in magnetic structure determination by neutron powder diffraction, *Physica B* **192**, 55 (1993).
- [47] J. Rodríguez-Carvajal, Recent developments of the program FullProf, newsletter commission powder diff. IUCr **26**, 12 (2001), https://www.iucr.org/_data/assets/pdf_file/0019/21628/cpd26.pdf.
- [48] J. Rodríguez-Carvajal, BASIREPS: A program for calculating irreducible representations of space groups and basis functions

- for axial and polar vector properties, *Solid State Phenomena* **170**, 263 (2011).
- [49] R. D. Shannon and C. T. Prewitt, Revised values of effective ionic radii, *Acta Crystallogr. B* **26**, 1046 (1970).
- [50] J.-W. Zhu, X.-X. Wang, C. Song, Q. Liu, J.-X. Sui, H.-D. Zhang, and Y.-Z. Long, Magnetic anisotropy and magnetization enhancement of Gd³⁺-doped SmFeO₃, *J. Magn. Magn. Mater.* **476**, 568 (2019).
- [51] I. Mikami, Paramagnetic behavior of rare-earth ions in some orthoferrites, *J. Phys. Soc. Jpn.* **34**, 338 (1973).
- [52] A. Bombik, B. Leśniewska, and A. W. Pacyna, Magnetic susceptibility of powder and single-crystal TmFeO₃ orthoferrite, *J. Magn. Magn. Mater.* **214**, 243 (2000).
- [53] Supplemental Material at <http://link.aps.org/supplemental/10.1103/PhysRevB.105.054407> for derivatives of magnetization curves versus temperature, and coercive field values versus composition and temperature.
- [54] R. Wolfe, R. D. Pierce, S. E. Haszko, and J. P. Remeika, Temperature-induced spin reorientation in rare earth orthoferrites—hysteresis loop studies, *Appl. Phys. Lett.* **11**, 245 (1967).
- [55] S. Yuan, Y. Wang, M. Shao, F. Chang, B. Kang, Y. Isikawa, and S. Cao, Magnetic properties of NdFeO₃ single crystal in the spin reorientation region, *J. Appl. Phys.* **109**, 07E141 (2011).
- [56] W. Sławiński, R. Przeniosło, I. Sosnowska, and E. Suard, Spin reorientation and structural changes in NdFeO₃, *J. Phys.: Condens. Matter* **17**, 4605 (2005).
- [57] G. Deng, P. Guo, W. Ren, S. Cao, H. E. Maynard-Casely, M. Avdeev, and G. J. McIntyre, The magnetic structures and transitions of a potential multiferroic orthoferrite ErFeO₃, *J. Appl. Phys.* **117**, 164105 (2015).
- [58] J. A. Leake, G. Shirane, and J. P. Remeika, The magnetic structure of thulium orthoferrite, TmFeO₃, *Solid State Commun.* **6**, 15 (1968).
- [59] S. Chaturvedi, P. Shyam, R. Bag, M. M. Shirolkar, J. Kumar, H. Kaur, S. Singh, A. M. Awasthi, and S. Kulkarni, Nano-size effect: Enhanced compensation temperature and existence of magnetodielectric coupling in SmFeO₃, *Phys. Rev. B* **96**, 024434 (2017).
- [60] S. K. Kulshreshtha and P. Raj, Spin-reorientation studies in the Fe_{1-x}Mn_xSn system (mossbauer study), *J. Phys. F* **10**, 1841 (1980).
- [61] A. McDannald, L. Kuna, M. S. Seehra, and M. Jain, Magnetic exchange interactions of rare-earth-substituted DyCrO₃ bulk powders, *Phys. Rev. B* **91**, 224415 (2015).
- [62] V. N. Derkachenco, V. A. Khokhlov, A. M. Kadomtseva, and M. M. Lukina, Magnetic properties of Tm_xDy_{1-x}FeO₃ single crystals, *Solid State Commun.* **16**, 393 (1975).
- [63] S. Cao, H. Zhao, B. Kang, J. Zhang, and W. Ren, Temperature induced spin switching in SmFeO₃ single crystal, *Sci. Rep.* **4**, 5960 (2015).
- [64] U. Staub, L. Rettig, E. M. Bothschafter, Y. W. Windsor, M. Ramakrishnan, S. R. V. Avula, J. Dreiser, C. Piamonteze, V. Scagnoli, S. Mukherjee, C. Niedermayer, M. Medarde, and E. Pomjakushina, Interplay of Fe and Tm moments through the spin-reorientation transition in TmFeO₃, *Phys. Rev. B* **96**, 174408 (2017).
- [65] K. R. S. Preethi Meher, A. Wahl, A. Maignan, C. Martin, and O. I. Lebedev, Observation of electric polarization reversal and magnetodielectric effect in orthochromites: A comparison between LuCrO₃ and ErCrO₃, *Phys. Rev. B* **89**, 144401 (2014).
- [66] M. Das and P. Mandal, Nonlinear magnetodielectric and magnetocaloric properties of double perovskite Ho₂FeCoO₆, *Physica B* **571**, 32 (2019).
- [67] R. Tackett, G. Lawes, B. C. Melot, M. Grossman, E. S. Toberer, and R. Seshadri, Magnetodielectric coupling in Mn₃O₄, *Phys. Rev. B* **76**, 024409 (2007).